Journal of Materials Science & Technology 93 (2021) 1–6

Contents lists available at ScienceDirect

Journal of Materials Science & Technology

journal homepage: www.elsevier.com/locate/jmst

Research Article

Properties and precipitates of the high strength and electrical conductivity Cu-Ni-Co-Si-Cr alloy

Yijie Ban[a,b,c,1], Yongfeng Geng[a,b,c,1], Jinrui Hou[a,b,c], Yi Zhang[a,b,c,*], Meng Zhou[a,b,c,*], Yanlin Jia[d,*], Baohong Tian[a,b,c], Yong Liu[a,b,c], Xu Li[e], Alex A. Volinsky[f]

[a] School of Materials Science and Engineering, Henan University of Science and Technology, Luoyang 471023, China
[b] Provincial and Ministerial Co-construction of Collaborative Innovation Center for Non-ferrous Metal New Materials and Advanced Processing Technology, Luoyang 471023, China
[c] Henan Key Laboratory of Nonferrous Materials Science and Processing Technology, Luoyang 471023, China
[d] School of Materials Science and Engineering, Central South University, Changsha 410083, China
[e] Center for Advanced Measurement Science, National Institute of Metrology, Beijing 100029, China
[f] Department of Mechanical Engineering, University of South Florida, 4202 E. Fowler Ave. ENG030, Tampa 33620, United States

ARTICLE INFO

Article history:
Received 4 February 2021
Revised 17 March 2021
Accepted 31 March 2021
Available online 8 May 2021

Keywords:
Copper
Mechanical properties
Precipitates
Deformation twins

ABSTRACT

In this paper, a novel Cu-1.5Ni-1.1Co-0.6Si-0.1Cr (wt.%) alloy with high strength and electrical conductivity was designed. After aging, excellent properties of 857±12 MPa yield strength, 300±8 HV microhardness, 42.8 ± 2.5% IACS conductivity, and 7 ± 0.5% elongation were obtained. According to the atomic structure, part of Ni atoms in Ni_2Si can be replaced by Co atoms to form nano-precipitates $(Ni, Co)_2Si$. The alloy's high strength and conductivity are mainly attributed to the fine and uniformly distributed $(Ni, Co)_2Si$ and Cr nano precipitates. The alloy strength was also enhanced by twins, dislocations, and grain refining strengthening. Based on the investigations of deformation microstructure and the orientation relationship between the $(Ni, Co)_2Si$ precipitates and the Cu matrix, the main reason for elongation increase is attributed to the formation of deformation twins and the small lattice mismatch strain at the coherent interfaces of precipitates and the Cu matrix.

1. Introduction

Designing copper alloys with high strength and electrical conductivity is important for improving efficiency and reducing waste in the electronics industry, specifically for lead-frames and electrical contacts [1–3]. At present, different copper alloys have been studied, including Cu-Be [4], Cu-Co-Si [5], Cu-Cr-Zr [6], Cu-Ag [7] and so on. Cu-Be alloy is one of the earliest studied alloy systems. Although it has excellent properties, the Cu-Be alloy has been replaced by other alloys due to the environmental hazards of Be. In addition, it is found that the strength and conductivity are lower than that of the Cu-Ni-Si alloy after studying the Cu-Co-Si alloy. For the Cu-Cr-Zr and Cu-Ag alloys, although they have excellent electrical conductivity, the strength can only reach 600 MPa, and the high price is also a troubling factor. Therefore, the high strength and conductivity Cu-Ni-Si alloy has been widely used in the electronics industry, such as C70275 and C70250 alloys, which have the strength of 600–900 MPa and the conductivity of 30–50%IACS. The methods for improving the alloy strength and conductivity have been explored by several researchers, and the introduction of the third element has been proven effective. For example, the addition of Zr can refine the structure and improve the electrical conductivity, but the mechanical properties of the alloy are sacrificed [8]. Ti addition can accelerate the aging response but unfortunately reduces the strength due to the agglomeration of precipitated phases [9]. Fine evenly distributed nanostructured precipitates formed during aging cause strong hardening of the alloy and recovered the electrical conductivity of the matrix by consuming solute atoms [10]. Therefore, it is very important to optimize the type and quantity of precipitates during aging. In recent years, the introduction of twins into copper has proven to be effective for improving strength and ductility. The twin boundary is a special coherent grain boundary, which hinders the movement of dislocations, just like the traditional grain boundary. For example, Lu et al. [11] obtained good tensile properties by introducing twin boundaries into Cu grains. Xue et al. [12] found that the introduction of nanoscale twins into the Cu-15Al alloy can improve

* Corresponding authors.
E-mail addresses: yizhang@haust.edu.cn (Y. Zhang), zhoumeng0902@126.com (M. Zhou), jiayanlin@126.com (Y. Jia).
[1] These authors contributed equally to this work.

https://doi.org/10.1016/j.jmst.2021.03.049
1005-0302/

its strength and ductility, reaching 700 MPa yield strength and 13% elongation at failure.

In this paper, deformation twins are introduced during cold deformation to further improve the properties of the alloy. In addition, the Co element was selected, and the introduction of Co has been proven to effectively improve the strength with no sacrifice of electrical conductivity. Krishna et al. [13] concluded that the strength and conductivity of the Cu-Ni-Si alloy can be improved by adding Co, which is attributed to the dispersion of Ni_2Si and Co_2Si phases. Co can partially replace Ni atoms, reducing the number of Ni or Co solute atoms in the Cu matrix. The addition of Co element can form orthorhombic (Ni, Co)$_2$Si precipitates sharing the same crystal system with Ni_2Si precipitates, and effectively reduce the Si composition in the Cu matrix, which means that there is less tendency of spin junction decomposition to fcc (Cu) + fcc (Si) [14]. Based on the original work [15–17], the Cu-2.4Ni-0.6Si alloy [18] has been designed with 700 MPa tensile strength, 210 HV hardness, and 45% IACS (International Annealed Copper Standard) conductivity. Another example is the Cu-4.0Ni-1.0Si alloy [19] with 704 MPa tensile strength and 48% IACS conductivity. When the content of the Ni and Si elements is higher than 8 wt.% and 1.8 wt.%, respectively, the strength can reach 1 GPa, but the conductivity is low, about 20% IACS. Therefore, the content choice of Ni, Co, and Si elements in this experiment is 1.5 wt.%, 1.1 wt.%, and 0.6 wt.%, respectively. The intention is to make Co and Ni form (Ni, Co)$_2$Si composite phase. In addition, the addition of Co can effectively inhibit the discontinuous precipitation, making the distribution of precipitates more uniform at the grain boundary and inside the grain [[20],[21]]. Cr is added to further optimize the alloy properties. Cr element has much less effect on the conductivity of the alloy compared with some other elements, such as Zr, Al, and Sn. Besides, the Cr particles can precipitate from the copper matrix during aging at medium temperature. Cr and (Ni, Co)$_2$Si particles enhance the strength of the alloy by dual-precipitation strengthening. Meanwhile, the addition of Cr can significantly refine the structure and improve the high temperature stability [[22],[23]].

In this work, the Cu-1.5Ni-1.1Co-0.6Si-0.1Cr alloy with high strength and electrical conductivity was designed. The strength of the alloy can reach 857 MPa and the conductivity is 42.8% IACS. It is worth noting that the elongation can reach 7%, which is 35% higher compared with the high strength and conductivity Cu-Ni-Co-Si alloy. This is mainly attributed to the coherent precipitates and the introduction of twins. The type and precipitates relationships of the Cu matrix in the alloy are analyzed in this paper, and a coherent relationship between precipitates and the matrix is obtained. It is found that the alloy strengthening is mainly due to precipitation strengthening, and the precipitates are also the main factors affecting the electrical resistivity.

2. Experimental procedures

The alloy with Cu-1.5Ni-1.1Co-0.6Si-0.1Cr (wt.%) composition was ingot-cast. After removing the surface defects, the ingot was homogenized at 1000 °C for 120 min, and then extruded into Φ35 mm cylinders. Solution treatment was performed at 900 °C for 2 h, followed by quenching in water. The cylinders were machined into 100 mm × 5 mm × 1 mm sheets and then deformed 50% at room temperature. Finally, the aging treatment was carried out in a tubular furnace at 400 °C, 450 °C, 500 °C, and 550 °C for 10 min, 20 min, 30 min, 60 min, 120 min, 240 min, and 480 min, respectively. Heat treatment was carried out under an argon protective atmosphere.

The microstructure was examined by using electron backscatter diffraction (EBSD) and transmission electron microscopy (TEM). The surface scratch of the EBSD sample was removed by mechanical polishing, and then electro-polishing was carried out for 1 min in a solution of 50% CH_3CH_2OH and 50% H_3PO_4 at a voltage of 5 V at 25 °C. The EBSD images were obtained by using a JMS-7800F field emission scanning electron microscope (SEM) with a step size of 0.5 μm and 20 kV voltage. The TEM sample was polished to 50 μm and then cut into a thin sheet with a diameter of 3 mm, and subsequently, ion thinned using Gatan 691 ion beam thinner. TEM and high-resolution TEM (HRTEM) experiments were carried out with an FEI Talos F200X and a JEM-2100 transmission electron microscope. Dog-bone tensile specimens with a gage cross-section of 12 mm × 2.25 mm were cut using electrical discharge machining (Fig. S1 in Supplementary Information). Uniaxial tensile tests were conducted at room temperature at the initial strain rate of 1×10^{-3} s^{-1}, with tensile direction parallel to the rolling direction. Vickers hardness measurements were performed on an HVS-1000 hardness tester, each sample was measured by five times, and the average hardness was recorded. Electrical conductivity was measured at a ZY9987 digital micro-ohm meter, and each sample was measured by three times.

3. Results and discussion

Fig. 1(a) shows the variation of the Cu-1.5Ni-1.1Co-0.6Si-0.1Cr alloy hardness aged at 500 °C. The hardness increases with aging time (under-aged stage), and the highest strength range is after 45–100 min (peaking-aged stage), and the highest hardness is 300 HV after 60 min of aging. Then, the hardness decreased gradually with aging time (over-aged stage). The supersaturated solid solution spontaneously decomposed in the aging process, forming new phases in the form of precipitates. It is well accepted that the increase in hardness in the under-aged stage can be attributed to the formation of primary precipitates and the decrease in the over-aged stage to the excessive growth of the precipitates. The hardness and conductivity under different aging time in this experiment can be seen in the supplement Fig. S2. Fig. 1(b) shows the comparison of tensile strength and conductivity of this work and various types of alloys. The Cu-1.5Ni-1.1Co-0.6Si-0.1Cr alloy designed in this work has combined high strength and electrical conductivity, and the product of strength and conductivity can reach 3.5 GPa•%IACS. To further study the precipitates of the alloy, we explored the precipitates at the best aging stage at 500 °C for 1 h.

Fig. 2 shows TEM images of the Cu-1.5Ni-1.1Co-0.6Si-0.1Cr alloy aged at 500 °C for 1 h. It can be seen from Fig. 2(a) that there are a lot of fine and uniformly distributed precipitates in the alloy with 12.7 nm size. The size distribution histogram of precipitates is shown in Fig. 2(a) with single peak distribution, which suggests no coarsening. The selected area diffraction pattern (SADP) along $[001]_{Cu}$ is shown in Fig. 2(b), and the orientation relationship (OR) between the matrix and the δ-(Ni, Co)$_2$Si phase at this point can be described as $[001]_{Cu}||[010]_{\delta}$ and $(110)_{Cu}||(001)_{\delta}$. The formation of (Ni, Co)$_2$Si is due to the similar lattice parameters, Ni_2Si: $a = 0.709$ nm, $b = 0.490$ nm and $c = 0.372$ nm, Pbnm (62) space group [27], Co_2Si: $a = 0.71$ nm, $b = 0.491$ nm, and $c = 0.378$ nm [28]. The quantitative energy dispersive spectra (EDS) results in Fig. 2(c) show that the atomic ratio of (Ni, Co) and Si is close to 2:1. According to the EDS analysis of the particles in Fig. 2(f–h), precipitates consist of Ni, Co, and Si, which also provides sufficient evidence for the existence of (Ni, Co)$_2$Si.

The crystal structure of Ni_2Si is orthorhombic with the Pbnm space group. Co atoms replace Ni atoms, and Fig. 3(a) shows the crystal structure of (Ni, Co)$_2$Si. Fig. 3(b) and (c) show the bright-field and dark-field TEM images, respectively. A large number of dislocations are entangled to form dislocation walls, and the precipitates are uniformly distributed in the Cu matrix. The distribution of precipitates is uniform, which is beneficial to improving the alloy strength and preventing cracking. The interaction between dislocations and precipitates can be seen in Fig. 3(d), and

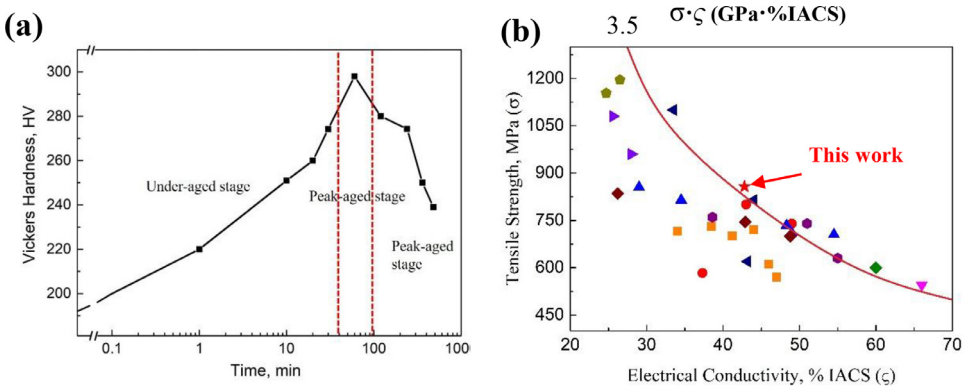

Fig. 1. (a) Variation of hardness with aging time for the Cu-1.5Ni-1.1Co-0.6Si-0.1Cr alloy aged at 500 °C; (b) Tensile strength and conductivity of this work and various types of alloys [24–26].

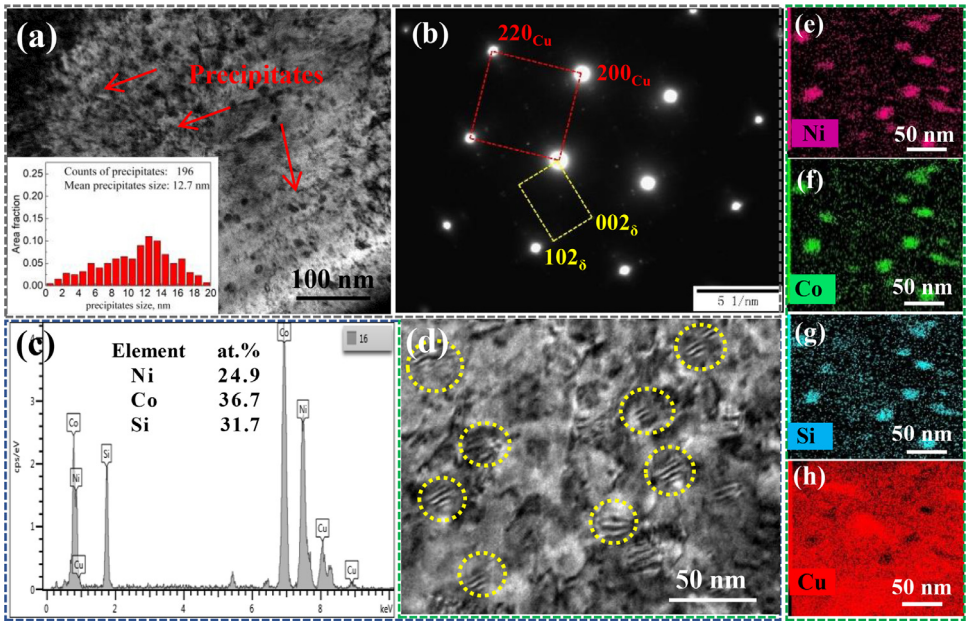

Fig. 2. Microstructures of the Cu-1.5Ni-1.1Co-0.6Si-0.1Cr alloy aging at 500 °C for 1 h. (a) Bright-field TEM images of the alloy; (b) beam direction of SADP along $[001]_{Cu}$; (c) EDS spectra of the δ-(Ni, Co)$_2$Si in (d); (d)–(h) BF TEM image, and EDS maps of the (Ni, Co)$_2$Si, respectively.

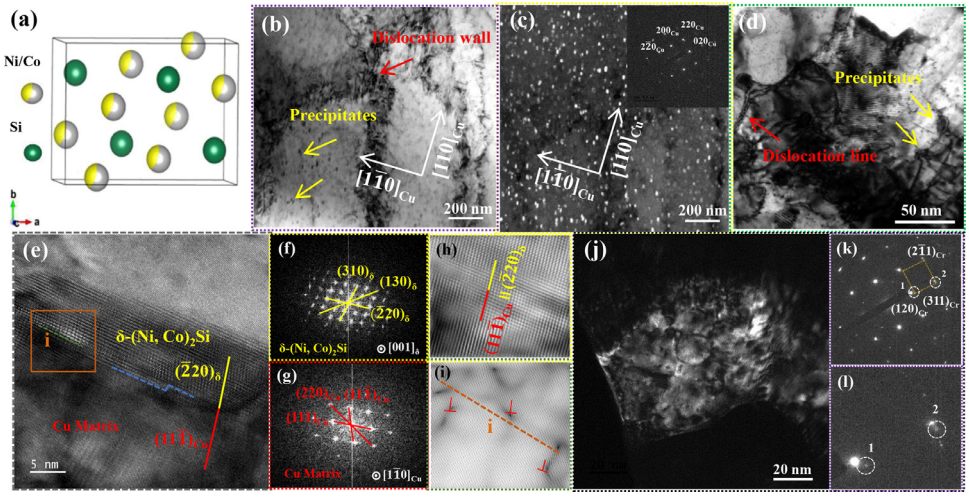

Fig. 3. HRTEM images and corresponding FFT patterns of the Cu-1.5Ni-1.1Co-0.6Si-0.1Cr alloy aged at 500 °C for 1 h: (a) crystal structure of (Ni, Co)$_2$Si; (b) bright-field TEM image; (c) dark-field TEM image; (d) nanoscale stacking faults; (e) HRTEM image taken from $[110]_{Cu}$, (f) FFT pattern of (Ni, Co)$_2$Si in (e); (g) FFT pattern of Cu matrix in (e); (h) HRTEM image of Cu matrix and (Ni, Co)$_2$Si boundary; (i) inversed FFT images of i region in (e); (j–l) bright-field images and SADP of Cr.

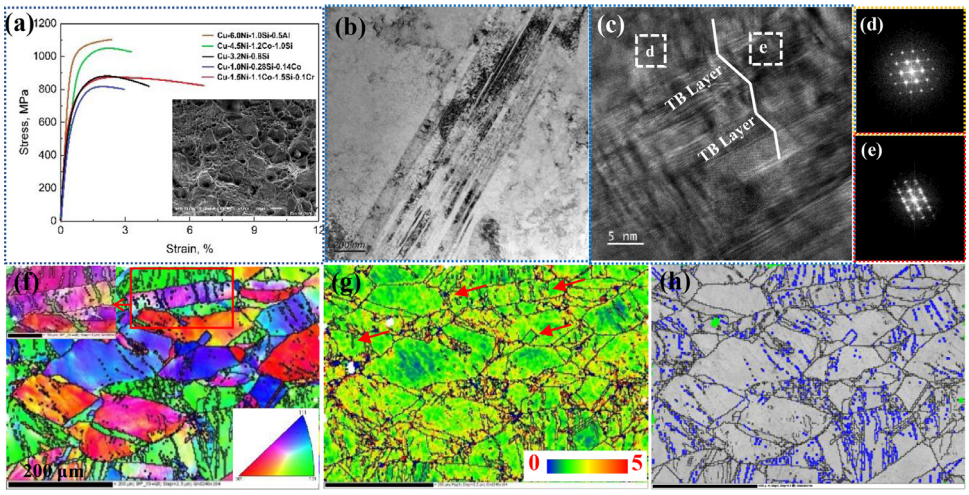

Fig. 4. (a) Stress-strain curves of the Cu-1.5Ni-1.1Co-0.6Si-0.1Cr alloy and Cu-Ni-Si-(*x*) alloys designed based on aging; (b) bright-field TEM images; (c) HRTEM image of TB layers; (d) and (e) FFT pattern of twins and Cu matrix; (f) EBSD image of Cu-1.5Ni-1.1Co-0.6Si-0.1Cr alloy aged at 500 °C for 1 h; (g) KAM map; (h) twin boundaries (TB) maps, where the blue lines are the twin boundaries.

the precipitates are distributed on the dislocations, which can effectively hinder the movement of dislocations. Fig. 3(e) shows the HRTEM image of the orientation relationship (OR) between the nanoscale (Ni, Co)$_2$Si and the Cu matrix aged at 500 °C for 1 h. The corresponding fast Fourier transform images (FFT) and inverse FFT (IFFT) images are shown in Fig. 3(f–g). The fully coherent interface between (Ni, Co)$_2$Si and Cu matrix could be observed when the incident beam is parallel to $[001]_{\delta}$ and $[1\bar{1}0]_{Cu}$ zone axes, as shown in Fig. 3(e). FFT of the Cu matrix and (Ni, Co)$_2$Si phase region was carried out, and the $(\bar{2}20)_{\delta}$ plane was found to be parallel to the $(11\bar{1})_{Cu}$ plane. In addition, based on the lattice parameters of (Ni, Co)$_2$Si and Cu, the interplanar spacing between the $(\bar{2}20)_{\delta}$ and $(11\bar{1})_{Cu}$ plane is about 0.204 nm and 0.208 nm, respectively. The lattice misfit was calculated as $\xi = (0.208-0.204)/(0.208+0.204) < 5\%$. The orientation relationship between the nanoscale (Ni, Co)$_2$Si phase and the Cu matrix could be described as $[001]_{\delta}||[1\bar{1}0]_{Cu}$ and $(\bar{2}20)_{\delta}||(11\bar{1})_{Cu}$ with a fully coherent interface. More coherent relations between precipitates and Cu matrix are provided in Fig. S3. Fig. 3(h) shows the HRTEM image of the Cu matrix and (Ni, Co)$_2$Si boundary. IFFT analysis of the region I (marked by orange square) in Fig. 3(e) shows that the coherent precipitates and the matrix have low lattice mismatch strain, as shown in Fig. 2(i). This means that the coherent interface between (Ni, Co)$_2$Si and Cu matrix can improve the strength without sacrificing plasticity. In addition, Cr precipitates were found in Fig. 3(j).

Fig. 4(a) shows the tensile strength and elongation of different Cu-Ni-Si-(*x*) alloys [[26],[29–31]]. Poor ductility is the main and most important problem for high-strength copper alloys. The alloy designed in this paper has good ductility and high strength, and the tensile strength is 857±12 MPa, and the elongation is 7 ± 0.5%. The illustration in Fig. 4(a) shows the typical fracture morphology of the Cu-1.5Ni-1.1Co-0.6Si-0.1Cr alloy, which is mainly composed of shallow dimples (2.1 μm) and large deep dimples (7.8 μm). This means that the fracture mechanism of this alloy is dimple fracture. The fracture mechanism of other alloys in Fig. 4(a) is a quasi-cleavage fracture. The main reasons are the coherent interfaces that possess a good atomic match between (Ni, Co)$_2$Si and the Cu matrix and the introduction of twins. In addition, Lu et al. [11] found that the strengthening effect of the twin boundaries is higher than that of the grain refinement when nano twins are introduced. The strengthening caused by twin boundaries can be quantified by the revised version of the traditional Hall-Petch grain boundary strengthening formula [32]:

$$\Delta\sigma_{TB} = V_{fT} \times K^{TB} \times \lambda_{TB}^{-\frac{1}{2}} \quad (1)$$

where V_{fT} is the volume fraction of twins, K^{TB} is a constant, and λ_{TB} is the average twin boundary spacing. It can be concluded that decreasing the twin spacing or increasing the volume fraction of twins enhances the strength.

Fig. 4(b) shows the distribution of deformation twins in the Cu-1.5Ni-1.1Co-0.6Si-0.1Cr alloy. It can be seen that the twins are continuous nanoscale twins, and the width of the twin layer is tens of nanometers. In addition, the twin layer of ~10 nm was found in Fig. 4(c). Fig. 4(d) and (e) show the FFT patterns of the Cu matrix and twins, respectively. EBSD was used to investigate the microstructure of the Cu-1.5Ni-1.1Co-0.6Si-0.1Cr alloy aged at 500 °C aged for 1 h in Fig. 4(f). Many twins were introduced into the alloy due to deformation, which is highlighted by blue lines in Fig. 4(h). According to the dislocation density in the twinned region, the twinned areas have much lower kernel average misorientation (KAM) values than the twin-free areas, which is indicated by the arrow in Fig. 4(g). The low internal dislocation density of the twins means that the twins are beneficial to releasing the local stress concentration and accommodates external stress [33]. Therefore, the activation of prolific internal twins is beneficial to preventing premature fracture and improve uniform elongation.

Multiple strengthening mechanisms are contributed to the high strength of the Cu-1.5Ni-1.1Co-0.6Si-0.1Cr alloy, including precipitation strengthening, work hardening, and grain refining strengthening. We evaluated the contribution of each mechanism for the alloy aged at 500 °C for 1 h.

Precipitation strengthening is the main strengthening mechanism of aged copper alloys. It is well known that the size and density of precipitates and the relationship between precipitates and dislocations have a great influence on the alloy strength. Generally, the relationship between precipitates and dislocations can be divided into two mechanisms: dislocation bypassing and particle shearing. The dislocation bypassing mechanism mainly occurs on the precipitates not coherent with the matrix. The shear mechanism usually occurs when the precipitates are coherent with the matrix [34]. At present, the (Ni, C_O)$_2$Si is widely recognized as a hard phase, and it is difficult for dislocations to shear precipitates. Therefore, the strengthening mechanism of the alloy is considered to be dislocation bypassing. The increase of yield strength caused by the bypassing mechanism (Orowan-Ashby equation) can be ex-

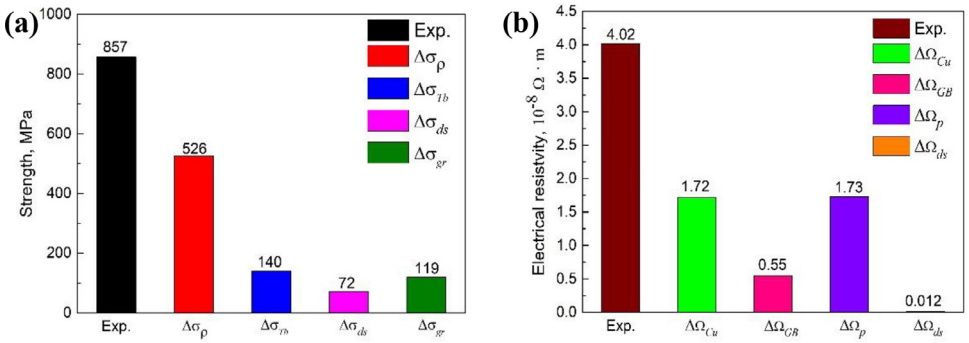

Fig. 5. (a) Strength and (b) electrical resistivity distribution histograms of the Cu-1.5Ni-1.1Co-0.6Si-0.1Cr alloy.

pressed as [35]:

$$\Delta_{\mathrm{p}} = 0.81 \cdot \frac{MGb}{2 \cdot \pi (1-\nu)^{\frac{1}{2}}} \cdot \frac{\ln\left(\frac{d_{\mathrm{precip.}}}{b}\right)}{\frac{1}{2} \cdot d_{\mathrm{precip.}} \cdot \sqrt{\frac{3\pi}{2f_{\mathrm{precip.}}}} - d_{\mathrm{precip.}}} \tag{2}$$

Here, M is the Taylor factor, $M = 3.06$, G is the shear modulus of copper, $G = 48$ GPa, ν is the Poisson's ratio, $\nu = 0.34$, b is the Burgers vector of Cu, $b = 0.2556$ nm, $d_{\mathrm{precip.}}$ is the average diameter of particles (~12.7 nm), and $f_{\mathrm{precip.}}$ is the volume fraction of precipitates (~5.9%) The contribution from the precipitation strengthening ($\Delta\sigma_{\mathrm{p}}$) is around 526 MPa. Grain refining strengthening can be expressed by the Hall-Petch formula [36]:

$$\Delta\sigma_{\mathrm{gr}} = f_{\mathrm{RX}} \frac{k}{\sqrt{d_{\mathrm{grain}}}} \tag{3}$$

Here, k is a constant of copper alloys, $k = 0.14$, f_{RX} is the volume fraction of the recrystallized region, and d_{grain} is the average diameter of grains (~0.4 μm). The contribution from the grain refinement strengthening ($\Delta\sigma_{\mathrm{g}}$) is around 118.6 MPa.

The alloy yield stress increase is attributed to increased dislocations density during cold deformation, and the value can be calculated by using the Taylor equation [37]:

$$\Delta\sigma_{\mathrm{ds}} = M\alpha Gb\sqrt{\rho} \tag{4}$$

where M is the Taylor factor, α is a geometric constant α=0.3, G is the shear modulus, b is the Burgers vector of copper, and ρ is the dislocation density. The dislocation strengthening effect mainly results from the geometrically necessary dislocations (GNDs). The density of GNDs can be calculated as [38]:

$$\rho = 2\theta/\mu b \tag{5}$$

Here, μ is the scanning step size (1 μm), θ represents the average local misorientation angle estimated based on the KAM maps from the EBSD analysis, which gives the dislocation density of 1.45 $\times$ 10^{14} m^{-2}, and the value caused by work hardening is 72 MPa. We can think of the strength brought by twins as: $\Delta\sigma_{\mathrm{TB}} = \Delta\sigma_{\mathrm{Exp.}} - \Delta\sigma_{\mathrm{p}} - \Delta\sigma_{\mathrm{gr}} - \Delta\sigma_{\mathrm{ds}}$, which is about 140 MPa, and the precipitation strengthening is the main strengthening mechanism of the Cu-1.5Ni-1.1Co-0.6Si-0.1Cr alloy, which can account for ~62%, and the strength distribution shown in Fig. 5(a).

For electrical conductivity properties, according to Matthiessen's rule [39], the electrical resistivity of the alloy is affected by the microstructure, including grain boundary, dislocation, and precipitates. The electrical resistivity can be written as:

$$\Omega = \Omega_{\mathrm{Cu}} + \Omega_{\mathrm{GB}} + \Omega_{\mathrm{Dis}} + \Omega_{\mathrm{p}} \tag{6}$$

where Ω_{Cu} is the electrical resistivity of the pure Cu (1.724 $\times 10^{-8}$ Ω m); Ω_{GB} and Ω_{Dis} are the resistivity induced by grain boundaries and dislocations, respectively; Ω_{p} is the resistance of the precipitates. The resistivity of grain boundary could be expressed as:

$$\Omega_{\mathrm{GB}} = \frac{2}{3}\Omega_{\mathrm{Me-GB}}\left(\frac{s}{v}\right) \tag{7}$$

where $\Omega_{\mathrm{Me-GB}}$ is the specific grain boundary electrical resistivity of Cu (2.04 $\times 10^{-16}$ Ω m^2) [40], $\frac{s}{v}$ is the grain boundary area per volume, taken to be $2.37/d_{\mathrm{grain}}$ if assuming that the grains are tetrakaidecahedral. The electrical resistivity caused by grain boundaries is calculated to be 0.55 $\times 10^{-8}$ Ω m and dislocation electrical resistivity is written as:

$$\Omega_{\mathrm{Dis}} = p\Omega_{\mathrm{pd}} \tag{8}$$

where Ω_{pd} is the specific dislocation electrical resistivity of Cu, taken to be 2.0 $\times 10^{-25}$ Ω m^3 [41], the dislocation density increases the resistivity of the alloy by 0.012 $\times 10^{-8}$ Ω m. The electrical resistivity caused by precipitates could be written as:

$$\Omega_{\mathrm{p}} = \Omega - \Omega_{\mathrm{Cu}} + \Omega_{\mathrm{GB}} + \Omega_{\mathrm{Dis}} \tag{9}$$

Therefore, the electrical resistivity caused by precipitation is 1.73 $\times 10^{-8}$ Ω m. The histogram of electrical resistivity distribution is shown in Fig. 5(b). It can be seen that the precipitates are the main factors affecting the electrical resistivity of the Cu-1.5Ni-1.1Co-0.6Si-0.1Cr alloy.

The Cu-1.5Ni-1.1Co-0.6Si-0.1Cr alloy designed in this experiment has high strength and high conductivity when being aged at 500 °C for 1 h, as shown in Fig. 1(b). For the precipitation strengthened copper alloy, the content of solute atoms in the matrix is the main factor affecting the electrical conductivity. The higher content of solute atoms can result in the greater scattering effect on electrons and the lower electrical conductivity [42]. With the increase of aging time, new precipitates were formed through the diffusion of solute atoms, which decreased the content of solute atoms in the matrix and increased electrical conductivity. The change of hardness is often divided into three intervals, as shown in Fig. 1(a). The highest strength is only in the peak aged state. Therefore, further optimization of deformation and aging can obtain better conductivity. In addition, when elements with the characteristics of high solubility in liquid Cu at high temperature or low solid solubility at room temperature, stable precipitates can be formed, which increases the conductivity of the alloy. A large number of $(Ni, Co)_2Si$ particles ensure the alloy's high hardness. In addition, Cr can significantly refine the grain, and further improve the electrical conductivity through the precipitation of Cr during aging at a medium temperature [22].

Many uniformly distributed (12.7 nm) and coherent nano precipitates were found in the alloy, which have a better precipitation strengthening effect. The precipitate strengthening mechanism of the Cu-1.5Ni-1.1Co-0.6Si-0.1Cr alloy was defined as the dislocation bypassing due to the hard particles. In addition, some reports indicate that the strengthening effect of the single mechanism is

not as effective as the cooperative effects of shearing and bypassing modes [43]. Several technologies are used to control the orientation relationship between the nano precipitates and the matrix to improve the strength, but the chaotic phase relationship often weakens the ductility [44]. Moreover, it is difficult to control the orientation of precipitates, which needs further experiments to explore.

Generally, excellent elongation and high strength are contradictory. Grain refinement is considered to be an effective method to improve strength and elongation, and it was found that the addition of Cr can effectively refine the grains in our previous work [22]. In addition, the introduction of deformation twins is also an effective method for grain refinement, because the introduction of twins can be regarded as reducing the grain size. In this paper, twins are introduced through the cold rolling deformation to further improve the alloy's ductility. The EBSD technique shows that the twinned areas have much lower kernel average misorientation (KAM) values than the twin-free areas. Therefore, by reducing the average internal dislocation density, the local pressure concentration can be effectively released and accommodates external stress.

Finally, the coherent interface between nano precipitate (Ni, $Co)_2Si$ and Cu matrix, and the low lattice mismatch strain mean that the alloy cannot easily crack during deformation. This means that the nanoscale (Ni, $Co)_2Si$ could provide a significant strengthening effect without sacrificing ductility, which also contributes to improving the high strength and high ductility of the alloy [45].

4. Conclusions

A novel Cu-1.5Ni-1.1Co-0.6Si-0.1Cr (wt.%) alloy with high strength and high conductivity was designed. Excellent properties were obtained after aging treatment, which included high yield strength of 857±12 MPa, the microhardness of 300±8 HV, the conductivity of 42.8 ± 2.5%%IACS, and excellent elongation of 7 ± 0.5%. During the aging process, a large number of fine and uniformly distributed nano-precipitates (Ni, $Co)_2Si$ and Cr were formed. The high strength of the alloy is attributed to the combined effect of work-hardening, grain refinement strengthening, precipitation strengthening, and the main strengthening mechanism of the alloy is precipitation strengthening. In addition, the formation of deformation twins and the small mismatch strain between the precipitates and Cu matrix provide good ductility of the alloy. The precipitates relationship was determined as: $[001]_\delta||[1\bar{1}0]_{Cu}$ and $(\bar{2}20)_\delta||(11\bar{1})_{Cu}$, or $[\bar{1}20]_\delta||[011]_{Cu}$, and $(002)_\delta||(1\bar{1}1)_{Cu}$.

Acknowledgments

This work was supported by the Open Cooperation Project of Science and Technology of the Henan Province (No. 182106000018), the Henan University Scientific and Technological Innovation Talent Support Program (No. 18HASTIT024), the National Natural Science Foundation of China (No. U1704143) and the National Natural Science Foundation of China (No. U1502274), Alex A. Volinsky acknowledges the support from the Government of the Russian Federation (2020–220–08–6662).

Supplementary materials

Supplementary material associated with this article can be found, in the online version, at doi:10.1016/j.jmst.2021.03.049.

References

[1] T. Hu, J.H. Chen, J.Z. Liu, Z.R. Liu, C.L. Wu, Acta Mater 61 (2013) 1210–1219.
[2] M.G. C, Electrical conductor alloy Electr World 89 (1) (1927) 137.
[3] S. Suzuki, N. Shibutani, K. Mimura, M. Isshiki, Y. Waseda, J. Alloys Compd. 417 (2006) 116–120.
[4] H. Tsubakino, R. Nozato, A. Yamamoto, Mater. Sci. 26 (1991) 2851–2856.
[5] Y.F. Geng, X. Li, H.L. Zhou, Y. Zhang, Y.L. Jia, B.H. Tian, Y. Liu, Alex A. Volinsky, X.H. Zhang, K.X. Song, G.X. Wang, L.H. Li, J.R. Hou, J. Alloys Compd. 842 (2019) 153518.
[6] J.Z. Li, H. Ding, B.M. Li, Mater. Sci. Eng. A 802 (2020) 140413.
[7] T. Varol, O. Güler, S.B. Akay, H.C. Aksa, Powder Technol 384 (2021) 236–246.
[8] W. Wang, H. Kang, Z. Chen, C. Zou, R. Li, G. Yin, T. Wang, Mater. Sci. Eng. A 673 (2016) 378–390.
[9] S. Suzuki, K. Hirabayashi, H. Shibata, K. Mimura, M. Isshiki, Y. Waseda, Scr. Mater. 48 (2003) 431–435.
[10] L. Lu, Y. Shen, L. Chen, K. Lu, Science 304 (2004) 422–426.
[11] K. Lu, L. Lu, S. Suresh, Science 324 (2009) 349–352.
[12] P. Xue, B.L. Xiao, Z.Y. Ma, Scr. Mater. 68 (2013) 751–754.
[13] S.C. Krishna, J. Srinath, A.K. Jha, B. Pant, S.C. Sharma, K.M. George, J. Mater. Eng. Perform. 22 (2013) 2115–2120.
[14] X.P. Xiao, Z.Y. Yi, T.T. Chen, R.Q. Liu, H. Wang, J. Alloys Compd. 660 (2016) 178–183.
[15] Z. Zhao, Y. Zhang, H.B. Tian, Y.L. Jia, Y. Liu, K.X. Song, A.A. Volinsky, J. Alloys Compd. 797 (2019) 1327–1337.
[16] J. Yi, Y.L. Jia, Y.Y. Zhao, Z. Xiao, K.J. He, Q. Wang, M.P. Wang, Z. Zhou, Acta Mater 166 (2019) 261–270.
[17] Y.F. Geng, Y.J. Ban, B.J. Wang, K.X. Song, Y. Zhang, Y.L. Jia, B.H. Tian, Y. Liu, A.A. Volinsky, J. Mater. Res. Technol. 9 (2020) 11918–11934.
[18] V.C. Srivastava, A. Schneider, V. Uhlenwinkel, S.N. Ojha, K. Bauckhage, J. Mater. Process. Technol. 147 (2004) 174–180.
[19] D. Li, Q. Wang, B. Jiang, W. Zhou, C. Dong, W. Hua, Q. Chen, Prog. Nat. Sci. 27 (2017) 467–473.
[20] M. Miki, Y. Ogino, Mater. Trans., JIM 35 (1994) 313–318.
[21] C.J. Guo, J.S. Chen, X.P. Xiao, H. Huang, W.J. Wang, B. Yang, J. Alloys Compd. 835 (2020) 155275.
[22] Y.J. Ban, Y. Zhang, Y.L. Jia, B.H. Tian, A.A. Volinsky, X.H. Zhang, Q.F. Zhang, Y.F. Geng, Y. Liu, X. Li, Mater. Des. 191 (2020) 108613.
[23] Y.J. Ban, Y. Zhang, B.H. Tian, K.X. Song, M. Zhou, X.H. Zhang, Y.L. Jia, X. Li, Y.F. Geng, Y. Liu, A.A. Volinsky, Mater. Character. 169 (2020) 110656.
[24] Q. Lei, Z. Li, T. Xiao, Y. Pang, Z.Q. Xiang, W.T. Qiu, Z. Xiao, Intermetallics 42 (2013) 77–84.
[25] W. Wang, E.Y. Gu, Z.N. Chen, H.J. Kang, Z.J. Chen, C.L. Zou, R.G. Li, G.M. Yin, T.M. Wang, Mater. Charact. 144 (2018) 532–546.
[26] Q. Lei, Z. Xiao, W.P. Hu, B.M. Derby, Z. Li, Mater. Sci. Eng. A 697 (2017) 37–47.
[27] K. Toman, The structure of Ni_2Si, Acta Crystallogr 5 (3) (1952) 329–331.
[28] S. Geller, V.M. Wolontis, Acta Crystallogr 8 (1955) 83–87.
[29] Z.L. Zhao, Z. Xiao, Z. Li, W.T. Qiu, H.Y. Jiang, L. Qian, Mater. Sci. Eng. A 759 (2019) 396–403.
[30] J. Li, G. Huang, L. Peng, Y. Kang, Materials (Basel) 12 (2019) 2076.
[31] J.Z. Huang, Z. Xiao, J. Dai, Z. Li, H.Y. Jiang, X.X. Zhang, Mater. Sci. Eng. A 744 (2019) 754–763.
[32] L. Ren, W.L. Xiao, D. Kent, M. Wan, C. Ma, L. Zhou, Scr. Mater. 184 (2020) 6–11.
[33] F. Yu, W.L. Xiao, D. Kent, M.S. Dargusch, J.S. Wang, X.Q. Zhao, C.L. Ma, Scr. Mater. 187 (2020) 285–290.
[34] W. Chen, J.Y. Zhang, S. Cao, Y. Pan, M.D. Huang, Q.G. Hu, Q.Y. Sun, L. Xiao, J. Sun, Acta Mater 117 (2016) 68–80.
[35] L. Wu, Nonlinear Anal 156 (2017) 167–196.
[36] Z. Wang, W. Lu, H. Zhao, C.H. Libscher, J.Y. He, D. Ponge, D. Qaabe, Z.M. Li, Sci. Adv. 6 (2020) 9543.
[37] T.H. Courtney, Mechanical Behavior of Materials, Waveland Press, 2005.
[38] D. Jorge-Badiola, A. Iza-Mendia, I. Gutiérrez, Mater. Sci. Eng. A 394 (2005) 445–454.
[39] A. Matthiessen, C. Vogt, Philos. Trans. R. Soc. London 154 (1864) 167–200.
[40] S.H. Pan, J. Yuan, P. Zhang, M. Sokoluk, G.C. Yao, X.C. Li, Appl Phys. Lett. 116 (2020) 014102.
[41] W. Zeng, J.W. Xie, D.S. Zhou, Z.Q. Fu, D.L. Zhang, E.J. Lavernia, J. Alloys Compd. 745 (2018) 55–62.
[42] S.H. Pan, Z.Y. Guan, G.C. Yao, X.C. Li, Curr. Appl. Phys. 19 (2019) 452–457.
[43] J. Buha, T. Ohkubo, Metall. Mater. Trans. A 39 (2008) 2259–2273.
[44] Z. Zeng, J.F. Nie, S.W. Xu, N. Birbilis, Nat. Commun. 8 (2017) 972.
[45] S.H. Jiang, H. Wang, Y. Wu, X.J. Liu, H.H. Chen, Z.P. Lu, Nature 544 (2017) 460–464.